informed consent prior to specimen collection, and the study was approved by the medical ethics committee.

DNA samples and dot blot analysis. Genomic DNA samples were collected from frozen surgical specimens or cultured cells using a QIAamp DNA Mini Kit (Qiagen, Tokyo, Japan) according to the manufacturer's instructions. Unmethylated, 5-mC-DNA and 5-hmC-DNA standard samples were purchased from Active Motif.

Genomic DNA samples were prepared in 0.1 M NaOH and denatured at 95°C for 5 min, then placed on ice, and neutralized with 0.1 volume of 6.6 M ammonium acetate. The samples were spotted onto Hybond-N+ nylon membrane (GE Healthcare, Tokyo, Japan), fixed with UV irradiation (Stratalinker 1800, auto crosslink-mode; Stratagene, Tokyo, Japan), washed, blocked with 5% skim milk, and incubated with anti-5-hmC antibody (1:10 000) or anti-5-mC monoclonal antibody (5 μg/mL; Calbiochem, Tokyo, Japan) at 4°C overnight, followed by incubation with species-specific HRP-conjugated secondary antibody (1:2000), and dot signal was visualized with the ECL Plus chemiluminescence assay kit (GE Healthcare). To ensure equal spotting of total DNA on the membrane, the same blot was stained with 0.02% methylene blue in 0.3 M sodium acetate (pH 5.2).

Quantitative real-time RT-PCR. Total RNA was extracted from cells using the Fast-Pure RNA Kit (Takara Bio, Shiga, Japan) or from clinical specimens using ISOGEN (Nippon Gene, Tokyo, Japan). Complementary DNA (cDNA) was synthesized

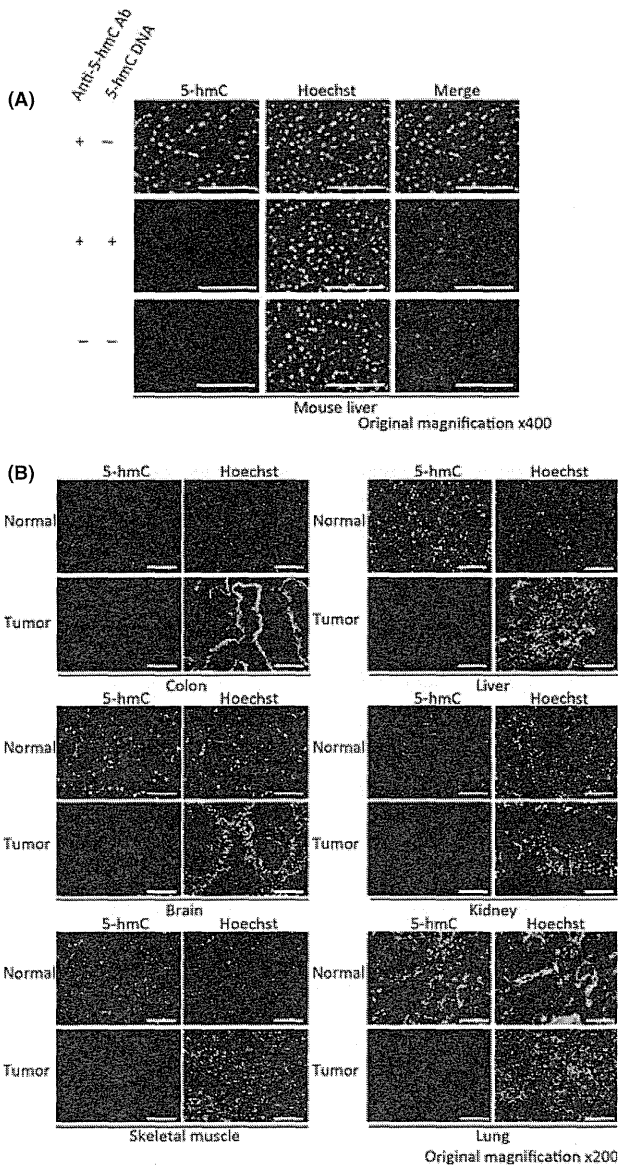

Fig. 1. Immunostaining of 5-hmC. Mouse liver tissues (A) and human tissue arrays (B) were stained with anti-5-hmC (green) antibody or Hoechst 33342 (blue). Scale bar: 100 μm.

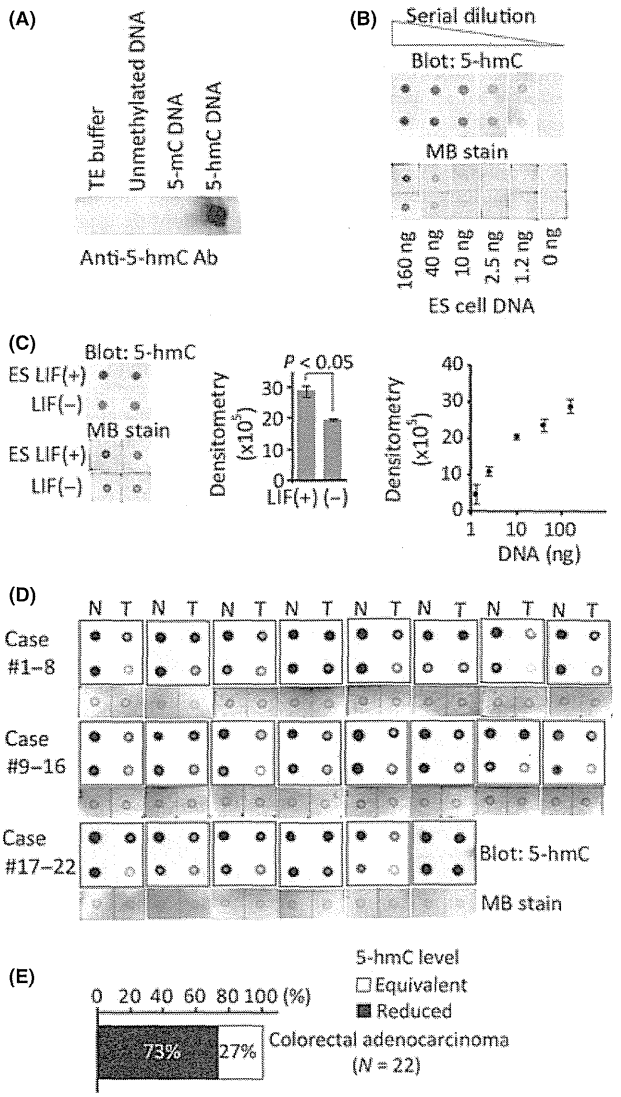

Fig. 2. Measurement of 5-hmC in colorectal cancers (CRCs). (A) Dot blot analysis using anti-5hmC antibody. (B) Genomic DNA from embryonic stem (ES) cells was subjected to dot blot. Loading control is shown by the methylene blue (MB) staining. Densitometry measurements against logarithmic DNA amount were plotted. (C) Quantitative assessment of 5-hmC in ES cell DNA (160 ng). ES cells were incubated with or without leukemia inhibitory factor (LIF) for 5 days. (D) Detection of 5-hmC in 22 pairs of clinical CRCs (T; right column on each membrane) and adjacent non-tumorous tissue (N; left) using dot blot. Twofold diluted DNA was also spotted in the second row on the same membrane. Loading control is shown by MB staining of undiluted DNA samples. (E) Classification of CRCs according to the 5-hmC level.

using the ImProm II reverse transcription system (Promega, Tokyo, Japan) and then subjected to quantitative RT-PCR with the ABI Prism 7000 Sequence Detection System (Applied Biosystems, Tokyo, Japan). The levels of gene expression were normalized in relation to that of *β-actin*. The PCR primer sequences are listed in Table S1.

Mutational analysis. Mutational analysis of *KRAS* exon1 and *BRAF* exon15 were performed using PCR (primers used to amplify those loci are described in Table S2) and direct sequencing methods as described previously.[31]

Cell lines and lentiviral-mediated *Tet1* knockdown. NIH3T3-BRAF^{V600E} cells were generated by transfection of human *BRAF*^{V600E}, as previously described.[32] Lentiviral short hairpin RNA vectors were purchased from Open Biosystems (Huntsville, AL, USA). NIH3T3 cells were infected with the virus according to the manufacturer's protocol and selected by puromycin.

Basic fibroblast growth factor treatment and immunoblot analysis. NIH3T3 cells were serum-starved for 24 h followed by basic fibroblast growth factor (bFGF; 1 μg/mL) stimulation for 30 min, and then lysed directly in Laemmli buffer. Blots were probed with anti-phospho-extracellular signal-regulated kinase (Erk) 1/2 (Thr202/Tyr204) or Erk1/2 antibodies (1:1000) followed by incubation with species-specific HRP-conjugated secondary antibodies (1:2000). Proteins were visualized using the ECL Plus chemiluminescence assay kit (GE Healthcare). The antibodies were obtained from Cell Signaling Technology (Beverly, MA, USA).

Soft agar colony formation assay. The lower layer of 0.5% agar in DMEM was placed in a 35-mm dish and permitted to solidify at room temperature. Then, 1.5×10^4 cells were suspended in the upper layer of 0.35% agar in DMEM containing 10% calf serum. The number of colonies over 50 μm was counted at 2 weeks after plating.

Statistical analysis. The results are presented as the means ± SEM. Associations were tested using the Student *t*-test and the Fisher exact test. $P < 0.05$ was considered statistically significant.

Results

Reduced 5-hydroxymethylcytosine in human tumor tissues. First, to examine the specificity of the antibody against 5-hmC, mouse liver tissues were stained with it. The signal was detected in the cell nuclei as expected, and the addition of 5-hmC-containing DNA to the reaction reduced the signal remarkably, indicating that the antibody specifically recognizes 5-hmC (Fig. 1A). Then, we performed immunostaining of human tumor and normal tissues. As shown in Figure 1(B), the signal of 5-hmC was scarcely detected in tumors compared to normal tissues, including colon, liver, brain, kidney, skeletal muscle and lung (Fig. 1B), suggesting that the loss of 5-hmC is a common phenomenon in tumorous tissues. We showed a representative photograph indicating the difference in the level of 5-hmC between the tumors and adjacent tissues derived from the mouse hepatic-tumor model (Fig. S1).[33]

Semiquantitative measurement of 5-hmC in gastrointestinal cancers. To evaluate the 5-hmC amount in many clinical specimens, the specificity of this antibody was also confirmed in blotting experiments (Fig. 2A). Serial dilution of genomic DNA extracted from mouse ES cells, in which a certain level of 5-hmC is detected,[14] were subjected to dot blot analysis. The good linearity between the signal density and DNA amount in a sufficient dynamic range supported the usefulness of this method for the quantification of 5-hmC in genomic DNA samples (Fig. 2B). Consistent with the previous report that the amount of 5-hmC decreases through differentiation in mouse ES cells,[14] the dot blot analysis demonstrated a significant loss of 5-hmC level in ES cells after withdrawal of leukemia inhibitory factor (LIF) (Fig. 2C).

Next, to assess the amount of 5-hmC in colorectal cancers (CRCs), clinical samples of human CRC obtained from surgical resection ($n = 22$ cases) were subjected to analysis. To compare the level of 5-hmC in tumors and the adjacent non-tumorous tissues, undiluted and twofold diluted DNA samples were spotted on the same membrane (Figs 2D,S2A). According to the dot blotting results, we classified the tumors into three groups: "5-hmC reduced" or "5-hmC increased" tumors were defined when the level of 5-hmC was 1/2-fold decreased (Fig. S2B) or twofold increased compared to the non-tumorous tissues, respectively. Others were classified into a "5-hmC equivalent" group (Fig. S2C). Notably, many of the CRC tumors (72.7% [16/22]) were included in the "5-hmC-reduced" group, with the others in the "5-hmC-equivalent" group (Fig. 2E). There was no distinct clinical features in 5-hmC-

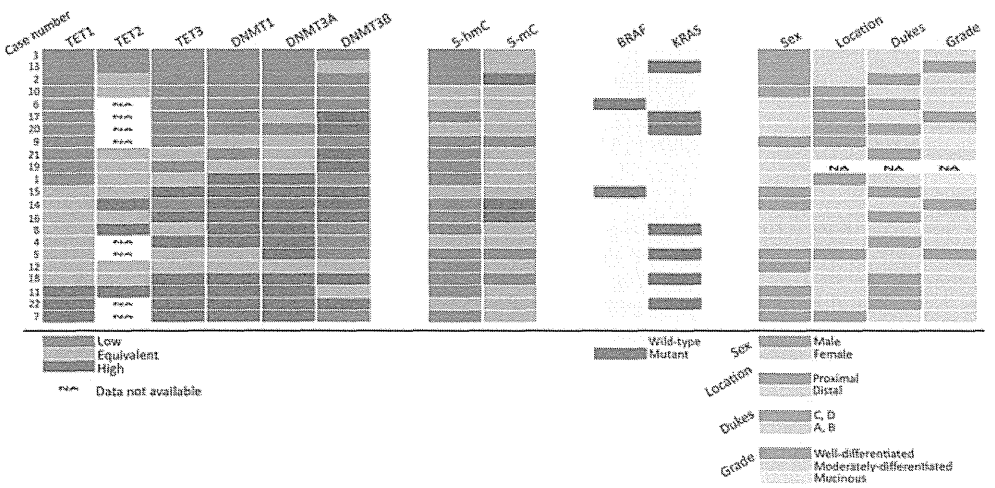

Fig. 3. Gene expressions, presence of mutations, and covariate status of 22 colorectal cancers (CRCs). Clinicopathological and molecular factors of 22 CRCs were displayed on a heat map representing *TET1*, *TET2*, *TET3*, *DNMT1*, *DNMT3A* and *DNMT3B* gene expression, and 5-hmC and 5-mC levels compared to adjacent background tissues. Presence of *BRAF* and *KRAS* mutations and covariate status of each tumor are also shown. Location: site of the primary tumor. Dukes: Dukes classification of the tumor. Grade: pathological tumor grade system.

doi: 10.1111/j.1349-7006.2012.02213.x

Table 1. Correlation between *TET1* gene expression and clinicopathological and molecular factors in colorectal cancer

Characteristics	Total $n = 22$	*TET1* expression		*P*-value
		Downregulated $n = 11$	Upregulated/ equivalent $n = 11$	
Age at surgery				
Mean ± SD (years)	65.3 ± 13.0	62.5 ± 13.4	67.8 ± 12.7	0.363
Range (years)	39–88	39–81	50–88	
Sex, *n* (%)				
Male	12 (54.5)	5 (45.5)	7 (63.6)	0.392
Female	10 (45.5)	6 (54.5)	4 (36.4)	
Site of tumor, *n* (%)				
Proximal	8 (38.1)	6 (60.0)	2 (18.2)	0.049
Distal	13 (61.9)	4 (40.0)	9 (81.8)	
Dukes grade, *n* (%)				
A, B	11 (52.4)	6 (60.0)	5 (45.5)	0.505
C, D	10 (47.6)	4 (40.0)	6 (54.5)	
Tumor grade, *n* (%)†				
Well diff	4 (19.0)	2 (20.0)	2 (18.2)	0.916
Moderately diff and mucinous	17 (81.0)	8 (80.0)	9 (81.8)	
KRAS exon 2, *n* (%)				
Wild-type	15 (68.2)	8 (72.7)	7 (63.6)	0.647
Mutant	7 (31.8)	3 (27.3)	4 (36.4)	
BRAF exon 15, *n* (%)				
Wild-type	20 (90.9)	10 (90.9)	10 (90.9)	1
Mutant	2 (9.1)	1 (9.1)	1 (9.1)	
TET2 gene expression, *n* (%)				
Downregulated	2 (14.3)	2 (28.6)	0 (0.0)	0.127
Upregulated or equivalent	12 (85.7)	5 (71.4)	7 (100)	
TET3 gene expression, *n* (%)				
Downregulated	10 (45.5)	9 (81.8)	1 (9.1)	**0.0006**
Upregulated or equivalent	12 (54.5)	2 (18.2)	10 (90.9)	
DNMT1 gene expression, *n* (%)				
Downregulated	8 (36.4)	8 (72.7)	0 (0.0)	**0.0004**
Upregulated or equivalent	14 (63.6)	3 (27.3)	11 (100)	
DNMT3A gene expression, *n* (%)				
Downregulated	7 (31.8)	6 (54.5)	1 (9.1)	**0.022**
Upregulated or equivalent	15 (68.2)	5 (45.5)	10 (90.9)	
DNMT3B gene expression, *n* (%)				
Downregulated	10 (45.5)	6 (54.5)	4 (36.4)	0.392
Upregulated or equivalent	12 (54.5)	5 (45.5)	7 (63.6)	
5-hmC level, *n* (%)				
Reduced	16 (72.7)	8 (72.7)	8 (72.7)	1
Equivalent	6 (27.3)	3 (27.3)	3 (27.3)	
5-mC level, *n* (%)				
Reduced or equivalent	19 (86.4)	10 (90.9)	9 (81.8)	0.534
Increased	3 (13.6)	1 (9.1)	2 (18.2)	

†Tumor grade: diff, differentiated. Significant *P*-values (< 0.05) are shown in bold.

reduced tumors; however, 63% (10/16) were located in the distal colon. These results were consistent with the finding that 5-hmC levels commonly decrease in neoplasms (Fig. 1B). The 5-hmC level was also reduced in the majority of gastric cancer specimens: 75% (9/12) (Fig. S3A,B).

Analysis of ten–eleven translocation (TET) and DNMT family genes expression in colorectal cancers. Given that the global level of 5-methylcytosine (5-mC) is frequently reduced in CRC tumors, we investigated whether the decrease in 5-hmC is simply due to the smaller amount of substrates, 5-mC. Then, the dot blot analysis using the anti-5-mC antibody was performed with the same sample sets applied to 5-hmC quantification, based on the specificity of the anti-5-mC antibody (Fig. S4A). Different from 5-hmC, the 1/2-fold decrease of 5-mC was detected in only 13.6% of cases (3/22), and the level of 5-mC was equivalent in most cases (72.7% [16/22]) (Fig. S4B, C). These findings indicate that the reduction of 5-hmC level in the CRC tumors is not always due to the lower amounts of 5-mC.

Recent studies indicate that the TET family of proteins can catalyze the conversion of 5-mC of DNA to 5-hmC in mammalian cells.[14,15] We suspected that the expression patterns of *TET* family genes or *DNMT* family genes encoding DNA methyltransferases affect the 5-hmC level in CRC samples. The expression of *TET1*, *2* and *3* and *DNMT1*, *3A* and *3B* was examined using quantitative real-time PCR. When we set a cut-off as twofold change, *TET1* expression was decreased in half of the tumors (50%[11/22]) and a large part of them (73% [8/11]) demonstrated less 5-hmC compared to the adjacent tissues (Fig. 3). We found that *TET2* mRNA expression was very

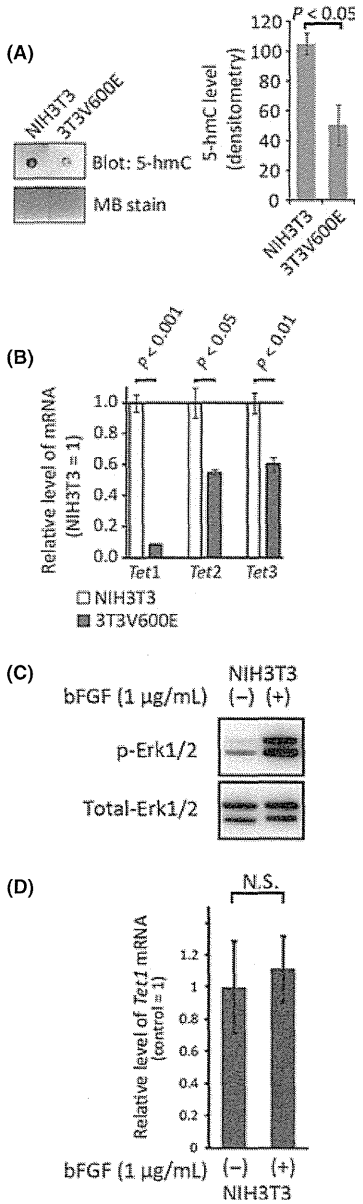

Fig. 4. 5-hmC levels and ten–eleven translocation (TET) genes expression in transformed NIH3T3 cells. (A) Genomic DNA (20 ng) of wild-type (NIH3T3) and transformed (3T3V600E) cells were subjected to dot blot analysis for 5-hmC detection. Methylene blue (MB) staining is used for DNA loading control. The graph shows the average of signals of three independent experiments. (B) Quantification of *Tet* family genes expression using quantitative RT-PCR in NIH3T3 cells and 3T3V600E cells. n = 3/each group. (C) Phosphorylation of Erk1/2 and (D) *Tet1* gene expression in response to bFGF stimulation for 30 min on NIH3T3 cells. NS, not significant. n = 3/each group.

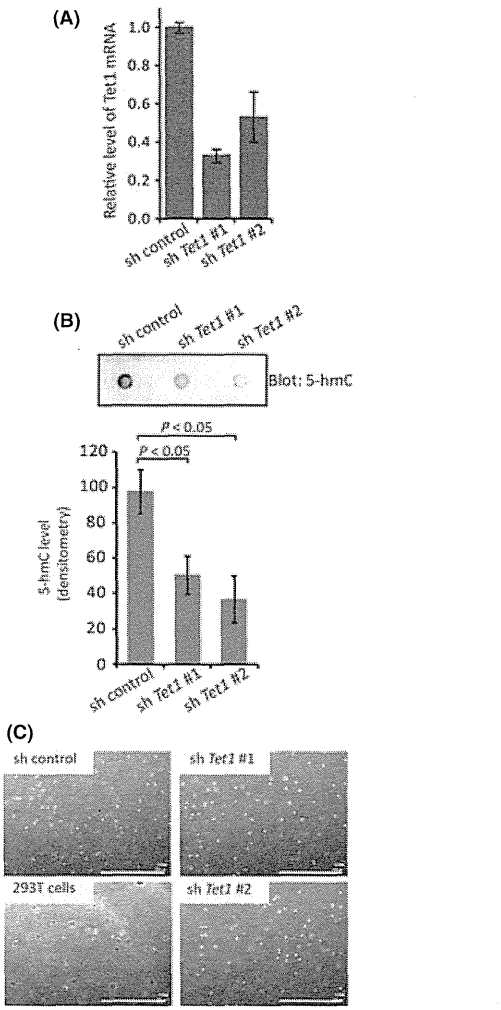

Fig. 5. Colony formation assay on *Tet1* stably knockdowned NIH3T3 cells. (A) Knockdown of *Tet1* in NIH3T3 cells was confirmed at mRNA levels. (B) 5-hmC levels in *Tet1*-depleted NIH3T3 cells (sh *Tet1* #1 and #2) were determined by dot blot and quantified by densitometry. n = 3/each group. (C) Neither line of *Tet1*-depleted NIH3T3 cells acquired colony forming ability. 293T cells were used as positive control for colony formation. Scale bar, 1 mm.

little both in CRC tumors and non-tumorous tissues, and that reduced *TET1* expression was tightly associated with decreased *TET3* mRNA ($P < 0.0006$) (Table 1). In contrast, most of 5-hmC-reduced tumors without *TET1* gene downregulation showed enhanced expression of *DNMT* genes (88%[7/8]) (Fig. 3). Although the reason why the upregulation of *DNMT* genes is associated with the loss of 5-hmC is unknown, it is likely that various mechanisms, including suppression of *TET1*, affect the level of 5-hmC in CRC tumors.

Next, we examined the expression level of genes implicated in the removal of 5-hmC. Poly ADP-ribose polymerase 1 (PARP1) and APEX1 are critical components of base excision repair (BER), and activation-induced cytidine deaminase and apolipoprotein B mRNA editing enzyme, catalytic polypeptide-like 2 (APOBEC2) are deaminases, of which overexpression are reported to enhance demethylation of 5-hmC.[20] As a result, the expression of *APEX1* gene was relatively, but not statistically, high in the tumors with low levels of 5-hmC (Fig. S5).

Reduced *Tet1* expression during cellular malignant transformation. Our data in clinical samples indicated a possibility that reduced 5-hmC is associated with malignant transformation. To address this notion, we performed an *in vitro* assay using NIH3T3 cells. We previously reported that the NIH3T3 cells stably expressing oncogenic *BRAF* (V600E)

doi: 10.1111/j.1349-7006.2012.02213.x

(3T3V600E cells) acquire transformation capability.[32] In the 3T3V600E cells, the level of 5-hmC was significantly decreased when compared to control cells (Fig. 4A). The expression level of *Tet1*, *Tet2* and *Tet3* was also reduced in the 3T3V600E cells compared to the control cells (Fig. 4B). To exclude the possibility that the downregulation of these genes is directly caused by the activation of MAPK signaling itself, we treated NIH3T3 cells with bFGF and analyzed the expression of *Tet1* gene. As shown in Figure 4(C), the activity of MAPK was clearly enhanced by the treatment of bFGF; however, the expression of *Tet1* was not affected (Fig. 4D). These findings indicated that the level of *Tet1* mRNA and 5-hmC was decreased in the process of cellular transformation in NIH3T3 cells.

Reduced *Tet1* expression itself is not sufficient for cellular transformation. The above data encouraged us to expect that the decrease of Tet1 plays a certain role in the mechanism of cellular transformation. Then, to examine whether the loss of Tet1 is sufficient for cellular transformation, we established *Tet1* stably knockdowned NIH3T3 cells (Tet1KD NIH3T3 cells) using lentiviral-vector shRNA (Fig. 5A). Tet1KD NIH3T3 cells showed a decreased 5-hmC level compared to control cells (Fig. 5B). When the Tet1KD NIH3T3 cells were applied to colony formation assay, the cells did not demonstrate the colony-forming ability (Fig. 5C), suggesting that the suppression of only *Tet1* mRNA is not enough for oncogene-induced cellular transformation.

Discussion

A previous report showed that myeloid tumors with *TET2* gene mutations compromising the catalytic activity displayed lower levels of 5-hmC when compared to bone marrow samples from healthy controls.[26,27] The finding suggests a possibility that lower 5-hmC might be preferable for the emergence of leukemic cells. In solid tumors, one study revealed using immunohistochemistry that 5-hmC levels were reduced in the carcinomas of prostate, breast and colon;[30] however, the analysis using commercial tissue arrays did not compare the 5-hmC level between tumors and adjacent normal tissues. Here, we provided confirmatory evidence of 5-hmC loss in solid cancers by analyzing paired matched tissues. Also, we established the semi-quantitative assay for 5-hmC using dot blotting.

Based on data from HPLC, global hypomethylation of cytosine is widely accepted as a characteristic of malignancies, including CRC.[1,2] Since this study was based on the dot blot technique with a relatively narrow window of sensitivity, the difference in global 5-mC level might be barely observed (Fig. S4B,C). Nonetheless, the difference in 5-hmC level was obvious in most of the tumors, suggesting that loss of 5-hmC is not just a secondary effect of global DNA hypomethylation in tumors. So far, the mutation of TET family genes abrogating the demethylating activity has not been found in solid cancers;[34] however, our data suggest that there are mechanisms causing loss of 5-hmC in solid tumors.

As a mechanism for loss of 5-hmC in CRC, we demonstrated the downregulation of *TET* genes (Fig. 3 and Table 1). This is reasonable because they encode the proteins catalyzing the conversion from 5-mC to 5-hmC. Our data also suggest the existence of another mechanism underlying the 5-hmC reduction because only half of CRC showed low expression of *Tet* mRNA. The other tumors demonstrated higher expression of *DNMT* genes. One possibility is that DNMT proteins functionally compete with TET proteins on DNA strands as reported.[35] IDH1 and IDH2 generate α-ketoglutarate, on which TET depend for their enzymatic activity. *IDH* mutations specifically produce 2-hydroxylglutarate and impair the TET2 catalytic function in leukemic cells.[36] The mutant *IDH1* and *IDH2* existed exclusively with *TET2* loss-of-function mutations in acute myeloid leukemia, which suggested that the mutations of their genes are functionally similar.[36,37] Therefore, it is likely that *IDH* mutants, which are also found in CRC,[38] induce the loss of 5-hmC regardless of the normal level of *TET* genes.

In addition, we cannot exclude the possibility that elimination of 5-hmC is enhanced by the active growth of cancer cells.[22] It is possible that enhanced proliferation leads to a "passive" 5-hmC reduction because the maintenance of methylcytosine catalyzed via DNMT1 is prevented by hydroxymethylation of the target cytosine.[39] Moreover, it is reported that BER proteins and the AID/APOBEC family mediate the demethylation of 5-hmC,[20,21] and that 5-hmC is further oxidized to 5-formylcytosine or 5-carboxylcytosine by TET proteins.[17,18] We cannot exclude the possibility that the increased expression of *APEX1* mRNA is implicated in the reduction of 5-hmC in tumor cells (Fig. S5), and we intend to analyze this possibility in future research.

Our *in vitro* data demonstrated that *TET1* was downregulated in the process of cellular transformation. Given the reports that TET1 is involved in the decision of ES cell lineage specification,[15,16] the downregulation of TET1 might achieve epigenetic profiles favorable for transformation. It is not clear whether TET function is always dependent of DNA demethylating activity. Indeed, we demonstrated that tumors with low *TET* expression did not always show lower 5-hmC. It is noteworthy that TET1 directly binds to transcriptional machinery,[40] and that TET can prevent DNMT activity without DNA demethylation.[35] Hence, it is still unknown whether TET1 can play roles in cellular transformation in the enzymatic activity-independent manner. Finally, the biological significance of the loss of 5-hmC in tumors remains to be elucidated; however, loss of 5-hmC could be a diagnostic marker for malignant transformation.

Acknowledgments

We thank Dr Teiji Motojima (Division of Abdominal Surgery, Motojima General Hospital, Gumma, Japan) and Dr Takaaki Sano (Division of Pathology, Motojima General Hospital) for providing human tissue specimens. We also thank Mitsuko Tsubouchi of our laboratory for technical assistance.

Disclosure Statement

The authors have no conflict of interest.

References

1 Feinberg AP, Vogelstein B. Hypomethylation distinguishes genes of some human cancers from their normal counterparts. *Nature* 1983; **301**: 89–92.
2 Gama-Sosa MA, Slagel VA, Trewyn RW *et al.* The 5-methylcytosine content of DNA from human tumors. *Nucleic Acids Res* 1983; **11**: 6883–94.
3 Jones PA, Baylin SB. The fundamental role of epigenetic events in cancer. *Nat Rev Genet* 2002; **3**: 415–28.
4 Herman JG, Baylin SB. Gene silencing in cancer in association with promoter hypermethylation. *N Engl J Med* 2003; **349**: 2042–54.
5 Ushijima T. Detection and interpretation of altered methylation patterns in cancer cells. *Nat Rev Cancer* 2005; **5**: 223–31.
6 Jones PA, Laird PW. Cancer epigenetics comes of age. *Nat Genet* 1999; **21**: 163–7.
7 Baylin SB, Herman JG. DNA hypermethylation in tumorigenesis: epigenetics joins genetics. *Trends Genet* 2000; **16**: 168–74.

8 Herman JG. Hypermethylation of tumor suppressor genes in cancer. *Semin Cancer Biol* 1999; **9**: 359–67.
9 Ushijima T, Nakajima T, Maekita T. DNA methylation as a marker for the past and future. *J Gastroenterol* 2006; **41**: 401–7.
10 Sun L, Hui AM, Kanai Y, Sakamoto M, Hirohashi S. Increased DNA methyltransferase expression is associated with an early stage of human hepatocarcinogenesis. *Jpn J Cancer Res* 1997; **88**: 1165–70.
11 Peng DF, Kanai Y, Sawada M *et al.* Increased DNA methyltransferase 1 (DNMT1) protein expression in precancerous conditions and ductal carcinomas of the pancreas. *Cancer Sci* 2005; **96**: 403–8.
12 Nakagawa T, Kanai Y, Saito Y, Kitamura T, Kakizoe T, Hirohashi S. Increased DNA methyltransferase 1 protein expression in human transitional cell carcinoma of the bladder. *J Urol* 2003; **170**: 2463–6.
13 Ley TJ, Ding L, Walter MJ *et al.* DNMT3A mutations in acute myeloid leukemia. *N Engl J Med* 2010; **363**: 2424–33.
14 Tahiliani M, Koh KP, Shen Y *et al.* Conversion of 5-methylcytosine to 5-hydroxymethylcytosine in mammalian DNA by MLL partner TET1. *Science* 2009; **324**: 930–5.
15 Ito S, D'Alessio AC, Taranova OV, Hong K, Sowers LC, Zhang Y. Role of Tet proteins in 5mC to 5hmC conversion, ES-cell self-renewal and inner cell mass specification. *Nature* 2010; **466**: 1129–33.
16 Koh KP, Yabuuchi A, Rao S *et al.* Tet1 and Tet2 regulate 5-hydroxymethylcytosine production and cell lineage specification in mouse embryonic stem cells. *Cell Stem Cell* 2011; **8**: 200–13.
17 Ito S, Shen L, Dai Q *et al.* Tet proteins can convert 5-methylcytosine to 5-formylcytosine and 5-carboxylcytosine. *Science* 2011; **333**: 1300–3.
18 He YF, Li BZ, Li Z *et al.* Tet-mediated formation of 5-carboxylcytosine and its excision by TDG in mammalian DNA. *Science* 2011; **333**: 1303–7.
19 Ooi SK, Bestor TH. The colorful history of active DNA demethylation. *Cell* 2008; **133**: 1145–8.
20 Guo JU, Su Y, Zhong C, Ming GL, Song H. Hydroxylation of 5-methylcytosine by TET1 promotes active DNA demethylation in the adult brain. *Cell* 2011; **145**: 423–34.
21 Cortellino S, Xu J, Sannai M *et al.* Thymine DNA glycosylase is essential for active DNA demethylation by linked deamination-base excision repair. *Cell* 2011; **146**: 67–79.
22 Inoue A, Zhang Y. Replication-dependent loss of 5-hydroxymethylcytosine in mouse preimplantation embryos. *Science* 2011; **334**: 194.
23 Kriaucionis S, Heintz N. The nuclear DNA base 5-hydroxymethylcytosine is present in Purkinje neurons and the brain. *Science* 2009; **324**: 929–30.
24 Szwagierczak A, Bultmann S, Schmidt CS, Spada F, Leonhardt H. Sensitive enzymatic quantification of 5-hydroxymethylcytosine in genomic DNA. *Nucleic Acids Res* 2010; **38**: e181.
25 Song CX, Szulwach KE, Fu Y *et al.* Selective chemical labeling reveals the genome-wide distribution of 5-hydroxymethylcytosine. *Nat Biotechnol* 2011; **29**: 68–72.
26 Delhommeau F, Dupont S, Della Valle V *et al.* Mutation in TET2 in myeloid cancers. *N Engl J Med* 2009; **360**: 2289–301.
27 Ko M, Huang Y, Jankowska AM *et al.* Impaired hydroxylation of 5-methylcytosine in myeloid cancers with mutant TET2. *Nature* 2010; **468**: 839–43.
28 Moran-Crusio K, Reavie L, Shih A *et al.* Tet2 loss leads to increased hematopoietic stem cell self-renewal and myeloid transformation. *Cancer Cell* 2011; **20**: 11–24.
29 Quivoron C, Couronne L, Della Valle V *et al.* TET2 inactivation results in pleiotropic hematopoietic abnormalities in mouse and is a recurrent event during human lymphomagenesis. *Cancer Cell* 2011; **20**: 25–38.
30 Haffner MC, Chaux A, Meeker AK *et al.* Global 5-hydroxymethylcytosine content is significantly reduced in tissue stem/progenitor cell compartments and in human cancers. *Oncotarget* 2011; **2**: 627–37.
31 Ohta M, Seto M, Ijichi H *et al.* Decreased expression of the RAS-GTPase activating protein RASAL1 is associated with colorectal tumor progression. *Gastroenterology* 2009; **136**: 206–16.
32 Ikenoue T, Hikiba Y, Kanai F *et al.* Functional analysis of mutations within the kinase activation segment of B-Raf in human colorectal tumors. *Cancer Res* 2003; **63**: 8132–7.
33 Kudo Y, Tanaka Y, Tateishi K *et al.* Altered composition of fatty acids exacerbates hepatotumorigenesis during activation of the phosphatidylinositol 3-kinase pathway. *J Hepatol* 2011; **55**: 1400–8.
34 Abdel-Wahab O, Mullally A, Hedvat C *et al.* Genetic characterization of TET1, TET2, and TET3 alterations in myeloid malignancies. *Blood* 2009; **114**: 144–7.
35 Xu Y, Wu F, Tan L *et al.* Genome-wide regulation of 5hmC, 5mC, and gene expression by Tet1 hydroxylase in mouse embryonic stem cells. *Mol Cell* 2011; **42**: 451–64.
36 Figueroa ME, Abdel-Wahab O, Lu C *et al.* Leukemic IDH1 and IDH2 mutations result in a hypermethylation phenotype, disrupt TET2 function, and impair hematopoietic differentiation. *Cancer Cell* 2010; **18**: 553–67.
37 Prensner JR, Chinnaiyan AM. Metabolism unhinged: IDH mutations in cancer. *Nat Med* 2011; **17**: 291–3.
38 Yen KE, Bittinger MA, Su SM, Fantin VR. Cancer-associated IDH mutations: biomarker and therapeutic opportunities. *Oncogene* 2010; **29**: 6409–17.
39 Valinluck V, Sowers LC. Endogenous cytosine damage products alter the site selectivity of human DNA maintenance methyltransferase DNMT1. *Cancer Res* 2007; **67**: 946–50.
40 Williams K, Christensen J, Pedersen MT *et al.* TET1 and hydroxymethylcytosine in transcription and DNA methylation fidelity. *Nature* 2011; **473**: 343–8.

Supporting Information

Additional Supporting Information may be found in the online version of this article:

Fig. S1. Immunostaining of 5-hmC in the genetic model of murine hepatic tumor.

Fig. S2. Definition and determination of 5-hmC or 5-mC level using dot blot analysis.

Fig. S3. Measurement of 5-hmC in human gastric cancers using dot blot.

Fig. S4. Measurement of 5-mC in colorectal cancer (CRC) using dot blot.

Fig. S5. Expression levels of genes encoding base excision repair proteins and cytidine deaminases of 22 colorectal cancers (CRC).

Table S1. Primer sequences for quantitative real-time PCR analysis.

Table S2. Primers for mutational analysis.

Please note: Wiley-Blackwell are not responsible for the content or functionality of any supporting materials supplied by the authors. Any queries (other than missing material) should be directed to the corresponding author for the article.

doi: 10.1111/j.1349-7006.2012.02213.x

J Gastroenterol (2012) 47:477–485
DOI 10.1007/s00535-011-0512-9

ORIGINAL ARTICLE—LIVER, PANCREAS, AND BILIARY TRACT

Value of post-vascular phase (Kupffer imaging) by contrast-enhanced ultrasonography using Sonazoid in the detection of hepatocellular carcinoma

Eriko Goto · Ryota Masuzaki · Ryosuke Tateishi · Yuji Kondo · Jun Imamura · Tadashi Goto · Hitoshi Ikeda · Masaaki Akahane · Shuichiro Shiina · Masao Omata · Haruhiko Yoshida · Kazuhiko Koike

Received: 17 August 2011 / Accepted: 20 November 2011 / Published online: 27 December 2011

Abstract
Background We evaluated the sensitivity and specificity of post-vascular phase (Kupffer imaging) by contrast-enhanced ultrasonography (CEUS) using perflubutane microbubbles (Sonazoid) in comparison with conventional B-mode ultrasonography (US) for the detection of hepatocellular carcinoma (HCC) nodules.
Methods A total of 100 treatment-naïve HCC patients admitted at our hospital between December 2007 and June 2009 were consecutively enrolled. The sensitivity and specificity of conventional and contrast-enhanced US were evaluated on a liver segment basis using dynamic CT as a reference standard. Movie files of conventional and enhanced US were stored separately for each segment (e.g., lateral, medial, anterior, and posterior) and reviewed randomly by two blinded readers.
Results A total of 138 HCC nodules (mean diameter 20.3 mm) were detected in 123 of 400 segments. Detection sensitivity of B-mode US was 0.837 for reader A and 0.846 for reader B, and that of CEUS was 0.732 for reader A and 0.831 for reader B. Specificity of B-mode US was 0.902 for reader A and 0.949 for reader B, and that of CEUS was 0.986 for reader A and 0.978 for reader B. CEUS false positives were mainly due to misidentification of hepatic cysts. A significant proportion of false-negative nodules are hyperechoic in B-mode US, likely because echogenicity hampers visualization of the defect in Kupffer imaging.
Conclusions Kupffer imaging by CEUS with Sonazoid showed very high specificity but rather mediocre sensitivity for HCC detection. CEUS is highly suitable for confirmatory diagnosis of HCC; however, caution should be exercised in reaching a diagnosis based only on CEUS.

Keywords Hepatocellular carcinoma · Contrast-enhanced ultrasonography · Sonazoid

Abbreviations

AFP	Alphafetoprotein
CEUS	Contrast-enhanced ultrasonography
Conventional B-mode US	Conventional B-mode ultrasonography
CT	Computed tomography
CTAP	CT during arterial portography
CTHA	CT during hepatic arteriography
CI	Confidence interval
Gd-EOB-DTPA	Gadolinium ethoxybenzyl diethylenetriamine pentaacetic acid
HBsAg	Hepatitis B surface antigen
HCC	Hepatocellular carcinoma
HCVAb	Hepatitis C virus antibody
MI	Mechanical index
STARD	The standards of reporting diagnostic accuracy

E. Goto · R. Masuzaki · R. Tateishi (✉) · Y. Kondo · J. Imamura · T. Goto · S. Shiina · H. Yoshida · K. Koike
Department of Gastroenterology, Graduate School of Medicine, The University of Tokyo, 7-3-1 Hongo, Bunkyo-ku, Tokyo 113-8655, Japan
e-mail: tateishi-tky@umin.ac.jp

H. Ikeda
Department of Clinical Laboratory, The University of Tokyo Hospital, Tokyo, Japan

M. Akahane
Department of Radiology, The University of Tokyo, Tokyo, Japan

M. Omata
Yamanashi Prefectural Hospital Organization, Kofu, Japan

SPIO-MRI	Superparamagnetic iron oxide in magnetic resonance imaging
US	Ultrasonography

Introduction

Hepatocellular carcinoma (HCC) is a common malignancy worldwide, the incidence of which is increasing in the USA and elsewhere [1–4]. Prognosis of HCC is poor unless the cancer is detected and treated at an early stage. HCC develops usually in a liver already suffering from some chronic disease, most commonly cirrhosis. Thus, early diagnosis of HCC is essential in the management of patients with chronic liver disease [5]. While initial screening for HCC is usually performed by ultrasonography (US), contrast-enhanced dynamic computed tomography (CT) is used in a confirmatory role. Hyperattenuation in the arterial phase with washout in the late phase on dynamic CT is considered a definite sign of HCC [6]. However, dynamic CT is accompanied by substantial X-ray exposure, and examination may be contraindicated by allergy to contrast material or renal dysfunction.

Sonazoid (Daiichi-Sankyo, Tokyo, Japan), a recently introduced ultrasonographic contrast agent that contains perflubutane microbubbles within a shell of phosphatidylserine (diameter 2–3 μm), has been widely used in Japan since 2007 [7, 8]. When injected intravenously, Sonazoid particles reach the liver in about 15 s, allowing the hepatic arterial vascularity to be visualized (vascular imaging). In addition, Sonazoid is taken up by Kupffer cells approximately 15 min after intravenous injection [post-vascular phase (Kupffer imaging)], which enables differentiation of benign and malignant nodules [9]. In contrast to some other ultrasonographic contrast agents, perflubutane microbubbles continue to resonate with moderate ultrasound pressure without collapsing. Thus, Kupffer imaging is stable for more than several hours, facilitating whole-liver scanning [10]. Several reports have suggested that contrast-enhanced ultrasonography (CEUS) with Sonazoid could detect HCC nodules that are not detectable by conventional B-mode US [11, 12]. These features of Sonazoid raise the possibility of one-step depiction and diagnosis of HCC using ultrasonography alone or surveillance of HCC solely by CEUS. We sought in the present study to evaluate the diagnostic ability of CEUS in Kupffer imaging using Sonazoid for HCC.

Patients and methods

Study populations

The study design was based on the principles described in the standards of reporting diagnostic accuracy (STARD) initiative [13]. A total of 100 treatment-naïve HCC patients who were admitted to the authors' institution for treatment between December 2007 and June 2009 were consecutively enrolled. Exclusion criteria were (1) patients with egg allergy or a past history of allergic reaction to Sonazoid; (2) those with HCC located in the caudate lobe; (3) those suffering severe cardiac or pulmonary dysfunction, which may affect Sonazoid delivery; and (4) those with HCC that showed an atypical dynamic CT pattern, as defined below. Data was collected prior to performance of Sonazoid CEUS.

This study was conducted according to the ethical guidelines for epidemiologic research of the Japanese Ministry of Education, Culture, Sports, Science and Technology and the Ministry of Health, Labour and Welfare. Informed consent was obtained from all patients. The study design was approved by the ethics committee of the authors' institution.

Computed tomography

HCC was diagnosed by using dynamic CT prior to enrollment; hyperattenuation in the arterial phase with washout in the late phase was considered diagnostic of HCC (Fig. 1a, b) [14]. Dynamic CT was performed less than 1 month before Sonazoid CEUS. All CT examinations were performed using a 64-detector row helical CT (Aquilion 64; Toshiba Medical, Tokyo, Japan and LightSpeed VCT; GE Health Care, Tokyo, Japan). All subjects were given an intravenous injection of nonionic contrast material at 2.0 mL/kg body weight, to a maximum of 100 mL, using a power injector (Dual Shot GX; Nemotokyorindou, Tokyo, Japan) at a rate of 3 mL/s. We used fixed scanning delays in the double-arterial phase protocol: the early arterial phase starts at 25 s, the late arterial phase at 40 s, and the equilibrium phase starts 120 s after the beginning of contrast material injection. Following this, a bolus-tracking program is used to optimize the scanning delay for dynamic imaging.

Ultrasonographic imaging

Ultrasonography was performed before initiation of treatment on an inpatient basis after at least 5 h fasting using the SSA-770A (Aplio; Toshiba, Tokyo, Japan) ultrasound apparatus. Tissue harmonic imaging (2.5/5.0 MHz, 14–27 Hz) was used in B-mode US, and Sonazoid CEUS employed phase-inversion harmonic mode [mechanical index (MI), 0.2–0.3; gain, 75–90 dB; dynamic range, 45 dB; frame rate, 15 frames/s). The focus point was set 8–10 cm from the body surface (Fig. 1c).

Ultrasonographic contrast media

For Sonazoid CEUS, one vial (16 μg) of Sonazoid (Daiichi-Sankyo, Tokyo, Japan) was reconstituted with 2 mL of

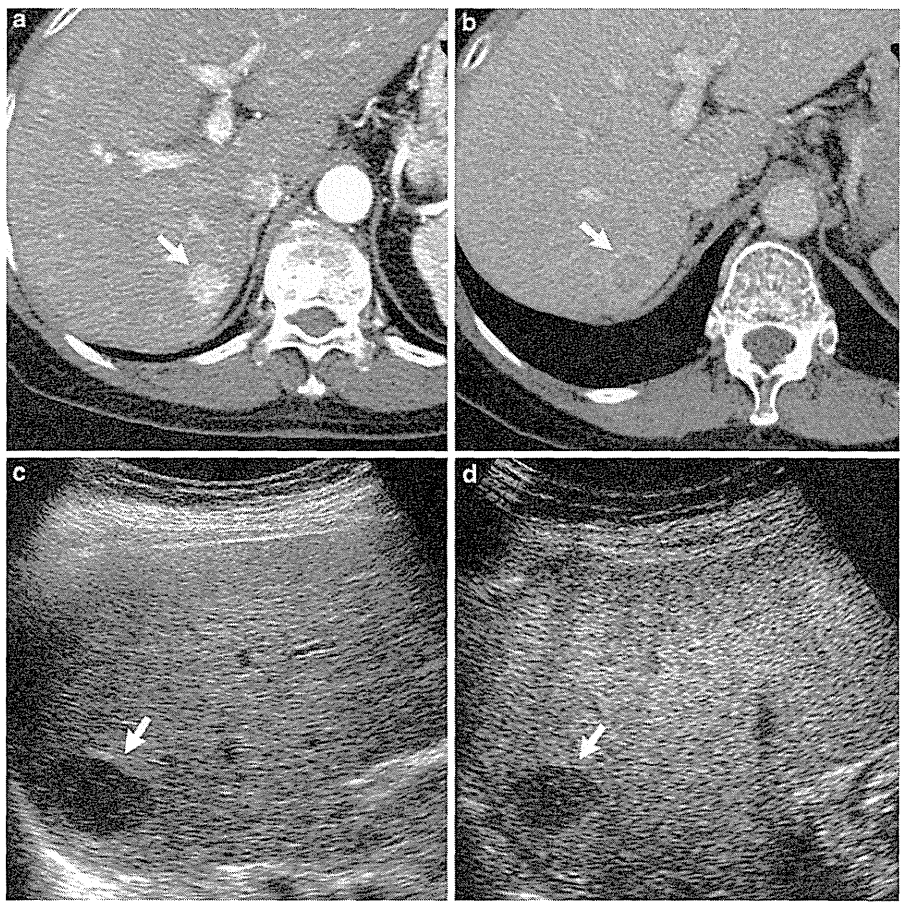

Fig. 1 Typical appearance of HCC (*arrow*) on dynamic CT and unenhanced and enhanced US. Appearance of HCC on dynamic CT [early enhancement (**a**) with late washout (**b**)]. The nodule was detected as a hypoechoic lesion by unenhanced US (**c**) and visualized as an enhancement defect in Kupffer imaging Sonazoid CEUS (**d**)

sterile water for injection, and 0.0075 mL/kg body weight of the solution was injected as a bolus via the antecubital vein and immediately flushed with 10 mL normal saline. Kupffer imaging was defined as the period starting 15 min after injection of Sonazoid (Fig. 1d).

Imaging technique and storage

US operators (EG, JI), each of whom had more than 8 years' experience in liver ultrasonography, were blinded with regard to subjects' clinical information including CT findings. All ultrasonographic images were recorded on movie files according to the following conditions. First, unenhanced ultrasonography was performed, and the images were stored in four separate movie files for each subject, one each for the left lateral, left medial, right anterior, and right posterior segments. Each segment was scanned from two directions in a standardized fashion, taking approximately 1 min. Sonazoid was then injected as described above, and after 15 min, Kupffer imaging scanning was performed and stored as for movie files. Vascular imaging images were not recorded. All movie files were formatted on uncompressed audio/video interleaving files with a resolution of 800 × 600 pixels and frame rate of 15 frames per second. Personal information was completely deleted from the movie files using the Toshiba Clip Washer ver. 3.5 software package (Toshiba Medical, Tokyo, Japan).

Movie file review

A total of 800 movie files, four each for unenhanced and Sonazoid-enhanced US per subject, were examined in a randomized order. Two readers (RT, RM), each of whom had more than 11 years' experience in liver ultrasonography, reviewed each movie file independently. The readers were blinded to all clinical and demographic information. After reviewing each movie file, the reviewers recorded the number of HCC nodules in the file, if any, and the confidence of diagnosis was graded on a four-point scale: 1, definitely absent; 2, probably absent; 3, probably present; 4, definitely present. The location of detected nodules and frame timestamp were also recorded.

After all movie files had been evaluated, the file order was restored. The evaluation by each reader was compared

with the findings of contrast-enhanced dynamic CT, using the latter as the reference standard. In some cases, nodules on a segment were also visualized in another movie file (e.g., a nodule in the medial segment was also visualized in a movie file for the anterior segment). In such cases, the third reader (EG) reassigned the score by referring to the readers' comments (e.g., "definitely present; however, the nodule seems to be located in the medial segment rather than the anterior segment"). In cases where two or more nodules were located in the same segment, the third reader assessed whether the first and second readers accurately pointed out the nodule in the same segment for nodule-based subgroup analysis according to the readers' comments.

To assess the characteristics of false-positive and -negative nodules, the third reader reviewed the corresponding movie files. Management of data regarding subject characteristics, scoring, and linking scores to randomized movie files was processed using Microsoft Access 2007 (Microsoft Corporation; Redmond, WA, USA).

Statistical analysis

Variables were expressed as mean ± standard deviations unless otherwise specified. Categorical variables were compared using Fisher's exact probability test. Sensitivity and specificity of unenhanced and enhanced US in the detection of HCC nodules were calculated using the presence or absence of HCC in the corresponding liver segment on dynamic CT as the reference standard. Confidence intervals were calculated based on the *F* distribution. We also calculated positive and negative likelihood ratios defined as sensitivity/(1 − specificity) and (1 − sensitivity)/specificity, respectively. Differences in proportion were assessed using Fisher's exact probability test. The concordance between the two readers was evaluated by weighted kappa statistics. The optimal cutoff in transforming the four-point scale to a dichotomous variable was validated by calculating the Youden index [15]. In addition to these segment-based analyses, tumor nodule-based analysis was also performed to evaluate tumor-associated factors that affected sensitivity for HCC detection. Statistical analyses were performed with S-plus ver. 7 (TIBCO Software, Inc., Palo Alto, CA, USA).

Results

Subject characteristics and CT findings

The study population consisted of 60 men and 40 women, with a mean age of 67.5 years. Seventy-seven subjects were hepatitis C virus antibody (HCVAb)-positive, and nine were hepatitis B surface antigen (HBsAg)-positive. During the study period, no treatment-naïve HCC patients were excluded, and only one patient refused to participate in the study. The total number of HCC nodules detected was 138, with a mean diameter of 23.1 ± 7.7 mm determined by dynamic CT. Subject characteristics are summarized in Table 1 [16]. A total of 10 segments had two and three segments had three HCC nodules. Thus, 123 of 400 segments (13 lateral, 11 medial, 63 anterior, and 36 posterior segments) were HCC-positive, whereas the other 277 were negative.

Evaluation of movie files

Weighted kappa statistics related to the concordance of evaluations between the two readers were 0.732 for B-mode US and 0.718 for CEUS, indicating fair reproducibility. In subsequent analyses, scores of one or two were considered as HCC absent, and three or four as HCC present according to Youden index analysis.

HCC detection sensitivity

HCC detection sensitivity was evaluated in the 123 segments that contained HCC nodules (Table 2). Sensitivities of B-mode US were 0.837 [95% confidence interval (CI) 0.761–0.893] by reader A and 0.846 (95% CI 0.770–0.899) by reader B. Sensitivities of Sonazoid CEUS were 0.732 (95% CI 0.646–0.803) and 0.831 (95% CI 0.681–0.831), respectively. Reader A correctly detected HCC on unenhanced ultrasonography, but failed to detect the corresponding nodule on Sonazoid CEUS in 23 segments, and reader B did so in 18 segments.

Table 1 Baseline characteristics ($n = 100$)

Variables	Value
Age (years)[a]	67.5 ± 10.6 (33–86)
Gender	
Male/female, *n* (%)/*n* (%)	60 (60.0)/40 (40.0)
Etiology	
HBsAg positive, *n* (%)	9 (9.0)
HCVAb positive, *n* (%)	77 (77.0)
Liver function	
Child-Pugh A/B, *n* (%)/*n* (%)	88 (88.0)/12 (12.0)
BMI (kg/m^2)[a]	23.3 ± 3.1 (17.7–34.4)
Number of tumor nodules (*n*)[a]	1.38 ± 0.79 (1–4)
Maximum diameter of tumor (mm)[a]	23.1 ± 7.7 (8–41)
Serum albumin concentration (g/dL)[a]	3.79 ± 0.6 (2.4–4.7)
Total bilirubin concentration (mg/dL)[a]	0.97 ± 0.44 (0.4–2.4)
AFP level >100 ng/mL, *n* (%)	15 (15.0)

BMI body mass index

[a] Data are expressed as mean ± SD (min–max)

Table 2 Sensitivity of HCC detection

	Conventional US			Sonazoid CEUS			*P* value
	Sensitivity		95% CI	Sensitivity		95% CI	
Reader A							
Total	0.837	(103/123)	0.761–0.893	0.732	(90/123)	0.646–0.803	0.062
Lateral	1.000	(13/13)	0.768–1.000	0.769	(10/13)	0.495–0.919	0.22
Medial	0.909	(10/11)	0.619–0.984	0.727	(8/11)	0.452–0.904	0.586
Arterial	0.841	(53/63)	0.731–0.912	0.714	(45/63)	0.592–0.812	0.133
Posterior	0.750	(27/36)	0.588–0.863	0.750	(27/36)	0.588–0.863	1.000
Reader B							
Total	0.846	(104/123)	0.770–0.899	0.756	(93/123)	0.672–0.824	0.110
Lateral	1.000	(13/13)	0.768–1.000	1.000	(13/13)	0.768–1.000	1.000
Medial	0.909	(10/11)	0.619–0.984	0.636	(7/11)	0.351–0.850	0.311
Arterial	0.857	(54/63)	0.749–0.923	0.746	(47/63)	0.625–0.838	0.179
Posterior	0.750	(27/36)	0.588–0.863	0.722	(26/36)	0.558–0.842	1.000

Numbers in parentheses indicate the number of segments considered as positive by a reader/number of segments with HCC by dynamic CT

Table 3 Factors affecting sensitivity

	Conventional US			Sonazoid CEUS		
	Sensitivity	95% CI	*P* value	Sensitivity	95% CI	*P* value
Size of tumor (*n*)						
<19 mm (69)	0.768	0.651–0.861	0.001	0.710	0.588–0.813	0.215
≥19 mm (69)	0.957	0.878–0.991		0.870	0.767–0.939	
Depth of tumor (*n*)						
<53 mm (69)	0.857	0.753–0.929	0.858	0.771	0.656–0.863	0.590
≥53 mm (69)	0.868	0.764–0.938		0.809	0.695–0.894	
BMI (*n*)						
<23 kg/m^2 (69)	0.855	0.750–0.928	0.805	0.800	0.683–0.884	0.834
≥23 kg/m^2 (69)	0.870	0.767–0.939		0.780	0.667–0.873	

Factors affecting sensitivity were assessed based on HCC nodules (total of 138 nodules). Continuous variables were divided by the median value. When the two readers disagreed, a nodule was considered detected when the averaged four-point scale score exceeded two. As shown in Table 3, sensitivity was significantly lower for small nodules (<19 mm) with B-mode US, and a similar trend was observed with Sonazoid CEUS. Neither nodule depth from body surface nor subject BMI had a significant effect on the sensitivity of either B-mode US or Sonazoid CEUS. We then assessed the B-mode US echo pattern of a total of 101 nodules correctly detected by both readers on B-mode US; eight nodules were hyperechoic; the remaining 93 were hypoechoic. The readers failed to detect 15 of these on Sonazoid CEUS. Of these, four were hyperechoic and 11 were hypoechoic on Sonazoid CEUS, suggesting that detection of a defect in Kupffer imaging by Sonazoid CEUS was relatively difficult when the nodule was hyperechoic on B-mode US ($P = 0.016$ by Fisher's exact test; Fig. 2).

HCC detection specificity

A total of 277 segments did not contain HCC nodules, as determined by dynamic CT. The readers' evaluation of movie files is summarized in Table 4. The specificity of B-mode US as evaluated by readers A and B was 0.902 (95% CI 0.861–0.932) and 0.949 (95% CI 0.917–0.970) and that of Sonazoid CEUS was 0.986 (95% CI 0.963–0.994) and 0.978 (95% CI 0.953–0.990), respectively. Sonazoid CEUS showed a higher specificity than B-mode US, irrespective of reader.

Both readers made a false-positive evaluation with Sonazoid CEUS in three segments, and one reader did so in five other segments. Of these eight segments, five had a cystic lesion (as shown by dynamic CT), which may have

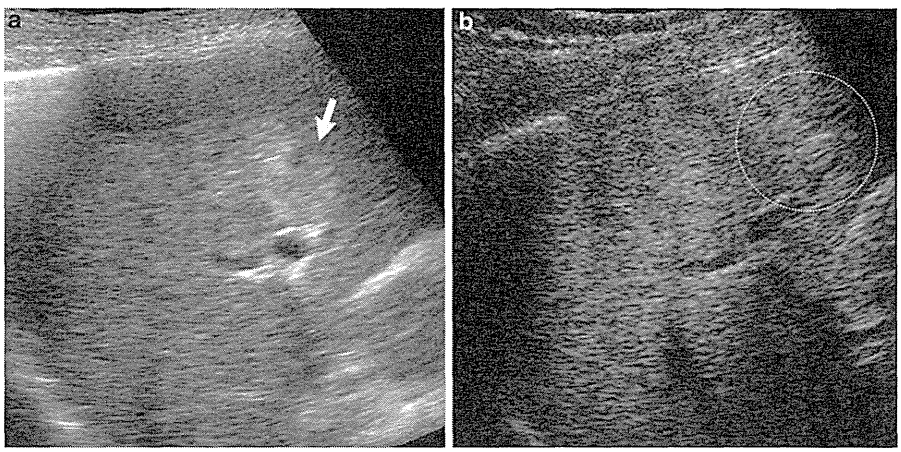

Fig. 2 A false-negative detected by Sonazoid CEUS. A hypervascular nodule was detected in segment 8. The nodule was visualized as a hyperechoic lesion (*arrow*) by unenhanced US (**a**), but disappeared (*circle*) after Kupffer imaging by Sonazoid CEUS (**b**)

Table 4 Specificity of HCC detection

	Conventional US			CEUS			*P*
	Specificity		95% CI	Specificity		95% CI	
Reader A							
Total	0.892	(247/277)	0.861–0.932	0.982	(272/277)	0.963–0.994	<0.001
Lateral	0.885	(77/87)	0.800–0.937	0.977	(85/87)	0.919–0.994	0.032
Medial	0.944	(84/89)	0.874–0.976	1.000	(89/89)	0.958–1.000	0.059
Arterial	0.865	(32/37)	0.718–0.941	0.973	(36/37)	0.860–0.995	0.199
Posterior	0.844	(54/64)	0.734–0.913	0.969	(62/64)	0.892–0.991	0.03
Reader B							
Total	0.949	(263/277)	0.917–0.970	0.978	(271/277)	0.953–0.990	0.109
Lateral	0.920	(80/87)	0.842–0.961	0.966	(84/87)	0.903–0.988	0.329
Medial	0.989	(88/89)	0.938–0.998	1.000	(89/89)	0.958–1.000	1.000
Arterial	0.919	(34/37)	0.785–0.972	0.946	(35/37)	0.821–0.985	1.000
Posterior	0.953	(61/64)	0.870–0.984	0.984	(63/64)	0.915–0.997	0.619

Numbers in parentheses correspond to the number of segments without HCC nodules by a reader/number of segments without HCC nodules by dynamic CT

been judged to be an enhancement defect in Kupffer imaging on Sonazoid CEUS (Fig. 3). Based on these sensitivities and specificities, the likelihood ratios for HCC presence when findings were positive were 11.4 and 43.4 with unenhanced and Sonazoid CEUS, respectively, and those for HCC presence when findings were negative were 0.171 and 0.222, respectively.

Discussion

The absence of Kupffer cells is one of the distinctive characteristics of hepatic malignant nodules, including HCC [8, 17]. This feature was first put to practical application for discriminating benign and malignant liver nodules using superparamagnetic iron oxide (SPIO) in magnetic resonance imaging (MRI) [18, 19]. Signal intensity of nodules on SPIO-MRI was reported to reflect grades of differentiation [20, 21]. The first-generation contrast agent Levovist (a suspension of galactose microparticle stabilized with palmitic acid) is also taken up by Kupffer cells in the liver and enables Kupffer cell imaging, similar to SPIO-MRI [22]. However, successful visualization of Kupffer cell defects by CEUS using Levovist requires sufficient ultrasound acoustic pressure to disrupt microbubbles. Repeated observation becomes impossible after microbubbles have been disrupted. This is a critical disadvantage in using Levovist CEUS for whole-liver screening. In contrast, Kupffer imaging using Sonazoid CEUS can be performed for several hours, which is suitable for imaging the entire liver.

In an assessment of the diagnostic accuracy of a test, evaluation of both sensitivity and specificity is essential. As an inverse correlation exists between sensitivity and

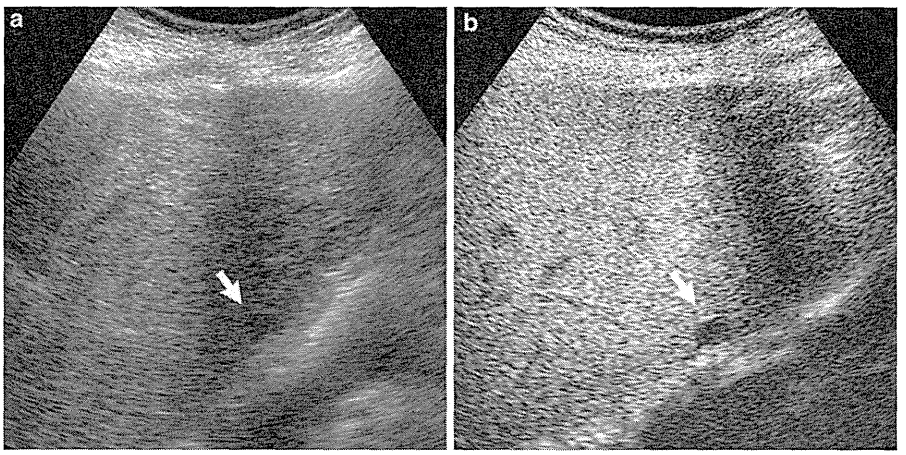

Fig. 3 A false-positive detected by Sonazoid CEUS. False-positive HCC detection by Sonazoid CEUS occurred mainly due to misrecognition of hepatic cysts (**a**, *arrow*) as HCC. Posterior enhancement was often obscured in Kupffer imaging by Sonazoid CEUS (**b**) and had an appearance (*arrow*) similar to that of an HCC nodule

specificity, reporting only sensitivity by recruiting those known to have the target disease is misleading and biased. Specificity of diagnostic imaging of liver nodules can be reported in at least three ways: (1) patient-, (2) segment-, or (3) nodule-based approaches. Calculation of specificity on a patient basis requires recruitment of individuals without HCC who undergo dynamic CT as a control. These controls should be patients with advanced liver fibrosis who are at a high risk for HCC. However, recruiting sufficient subjects to provide specificity with a narrow confidence interval is problematic. For a nodule-based study, controls should be benign nodules, such as hemangiomas, in patients with chronic liver disease. Previous reports on the diagnostic ability of Sonazoid CEUS on liver nodules were all based on this study design [11, 12, 23–26]. However, the diagnostic accuracy assessed by this type of study is appropriate for differential diagnosis, but not for detection. In the present study we adopted the second approach. Ultrasound movie files were obtained from patients with known HCC, but readers did not know whether each segment contained a cancer nodule, which made evaluation of specificity possible. This design had the additional advantage that matching ultrasonographic conditions such as parenchymal heterogeneous echogenicity or subjects' compliance was unnecessary, as "control" movie files were obtained from the same individuals. In addition, to reduce the likelihood of bias, ultrasound scanning of each segment was standardized, and B-mode US and Sonazoid CEUS movie files of the same segment were reviewed separately. These procedures were chosen for research purposes and obviously differ from clinical settings.

As a result, the sensitivity of Sonazoid CEUS for HCC detection was shown to be no greater than that of B-mode US. This may be due to several reasons. First, the lower acoustic power of Sonazoid CEUS compared with B-mode US (to avoid disrupting microbubbles) makes visualizing a deep nodule from the surface problematic. For enough sensitivity of CEUS, careful examination is demanded because CEUS is easily affected by the artifacts (such as bone and air) in low mechanical index (MI) mode. These artifacts were found especially in the right intercostal scan. Second, detection of nodules in obese patients is difficult due to attenuation of ultrasound by fatty tissue. However, subgroup analysis did not support this hypothesis. Hyperechoic nodules were unlikely to be detected by Kupffer imaging of Sonazoid CEUS, but this cannot entirely explain the low sensitivity. It should be noted that some nodules typical of HCC by dynamic CT are seen to possess Kupffer cells [27, 28]. However, Sonazoid CEUS can provide very stable post-vascular phase images for up to 60–120 min. Post-vascular phase obtained from later time (20–30 min) may increase the sensitivity of CEUS. The negative likelihood ratio of HCC presence by Sonazoid CEUS was insufficient, and thus caution should be taken when using this technique for diagnosis.

In contrast, the specificity of Sonazoid CEUS was shown to be about 98% irrespective of reader. The majority of false positives were due to misdiagnosis of cystic lesions as Kupffer imaging defects. Posterior enhancement, one of the major ultrasonographic characteristics of cystic lesions, may be obscured in Sonazoid CEUS. A positive likelihood ratio of at least 43 indicates that Sonazoid CEUS is suitable for confirmative diagnosis of HCC. Hyperechoic nodules were unlikely to be detected by post-vascular phase of Sonazoid US, but this cannot entirely explain the low sensitivity. Some new techniques can facilitate the diagnosis of tumor and should be combined with routine CEUS examination in clinical practice [29].

In clinical practice, US is performed in real time, so ambiguous lesions may be scrutinized by changing patients' positions and requesting that they hold their breath. Final diagnoses are likely to be based on findings obtained by both contrasted and B-mode US. Thus, the sensitivity and specificity obtained in this study may be

inferior to those in actual practice. Indeed, when movie files were re-examined 3 months after first review and images from both B-mode US and Sonazoid CEUS were examined simultaneously, the sensitivity improved compared to that for Sonazoid CEUS alone (data not shown). Other factors that may have affected HCC detectability were (1) that we did not use information in arterial images obtained by Sonazoid CEUS, which may have facilitated the assessment of the vascularity of targeted nodules; and (2) by using dynamic CT as the gold standard, atypical HCC detected with US may have been judged as false positives. The present study only included classical HCC and dynamic CT has its limitation. Early HCC is hypovascular on dynamic imaging in most cases. Its accurate diagnosis has remained difficult even with CT during hepatic arteriography (CTHA) and CT during arterial portography (CTAP). Gadolinium ethoxybenzyl diethylenetriamine pentaacetic acid (Gd-EOB-DTPA)-enhanced MRI should be considered regarding diagnosis of early HCC [30].

In conclusion, we have shown that Sonazoid CEUS detects HCC with high specificity, but its sensitivity is no higher than that of B-mode US. Sonazoid CEUS is more suitable for confirmative diagnosis of HCC and can be performed immediately after B-mode US for this purpose.

Conflict of interest The authors declare that they have no conflict of interest.

References

1. Llovet JM, Burroughs A, Bruix J. Hepatocellular carcinoma. Lancet. 2003;362(9399):1907–17.
2. Parkin DM, Bray F, Ferlay J, Pisani P. Global cancer statistics, 2002. CA Cancer J Clin. 2005;55(2):74–108.
3. El-Serag HB. Hepatocellular carcinoma: recent trends in the United States. Gastroenterology. 2004;127(5 Suppl 1):S27–34.
4. Colombo M, de Franchis R, Del Ninno E, Sangiovanni A, De Fazio C, Tommasini M, et al. Hepatocellular carcinoma in Italian patients with cirrhosis. N Engl J Med. 1991;325(10):675–80.
5. Makuuchi M, Kokudo N. Clinical practice guidelines for hepatocellular carcinoma: the first evidence based guidelines from Japan. World J Gastroenterol. 2006;12(5):828–9.
6. Bruix J, Sherman M, Llovet JM, Beaugrand M, Lencioni R, Burroughs AK, et al. Clinical management of hepatocellular carcinoma. Conclusions of the Barcelona-2000 EASL conference. European Association for the Study of the Liver. J Hepatol. 2001;35(3):421–30.
7. Yanagisawa K, Moriyasu F, Miyahara T, Yuki M, Iijima H. Phagocytosis of ultrasound contrast agent microbubbles by Kupffer cells. Ultrasound Med Biol. 2007;33(2):318–25.
8. Tanaka M, Nakashima O, Wada Y, Kage M, Kojiro M. Pathomorphological study of Kupffer cells in hepatocellular carcinoma and hyperplastic nodular lesions in the liver. Hepatology. 1996; 24(4):807–12.
9. Shunichi S, Hiroko I, Fuminori M, Waki H. Definition of contrast enhancement phases of the liver using a perfluoro-based microbubble agent, perflubutane microbubbles. Ultrasound Med Biol. 2009;35(11):1819–27.
10. Kindberg GM, Tolleshaug H, Roos N, Skotland T. Hepatic clearance of Sonazoid perfluorobutane microbubbles by Kupffer cells does not reduce the ability of liver to phagocytose or degrade albumin microspheres. Cell Tissue Res. 2003;312(1):49–54.
11. Hatanaka K, Kudo M, Minami Y, Maekawa K. Sonazoid-enhanced ultrasonography for diagnosis of hepatic malignancies: comparison with contrast-enhanced CT. Oncology. 2008;75(Suppl 1):42–7.
12. Moriyasu F, Itoh K. Efficacy of perflubutane microbubble-enhanced ultrasound in the characterization and detection of focal liver lesions: phase 3 multicenter clinical trial. AJR Am J Roentgenol. 2009;193(1):86–95.
13. Bossuyt PM, Reitsma JB, Bruns DE, Gatsonis CA, Glasziou PP, Irwig LM, et al. The STARD statement for reporting studies of diagnostic accuracy: explanation and elaboration. Ann Intern Med. 2003;138(1):W1–12.
14. The committee for revision of the clinical practice guidelines for hepatocellular carcinoma. Clinical practice guidelines for hepatocellular carcinoma—The Japan Society of Hepatology 2009 update. Hepatol Res. 2010;40(s1):16–47 (Practice Guideline).
15. Youden WJ. Index for rating diagnostic tests. Cancer. 1950;3(1): 32–5.
16. Thompson Coon J, Rogers G, Hewson P, Wright D, Anderson R, Cramp M, et al. Surveillance of cirrhosis for hepatocellular carcinoma: systematic review and economic analysis. Health Technol Assess. 2007;11(34):1–206.
17. Watanabe R, Matsumura M, Munemasa T, Fujimaki M, Suematsu M. Mechanism of hepatic parenchyma-specific contrast of microbubble-based contrast agent for ultrasonography: microscopic studies in rat liver. Invest Radiol. 2007;42(9):643–51.
18. Saini S, Stark DD, Hahn PF, Bousquet JC, Introcasso J, Wittenberg J, et al. Ferrite particles: a superparamagnetic MR contrast agent for enhanced detection of liver carcinoma. Radiology. 1987;162(1 Pt 1):217–22.
19. Stark DD, Weissleder R, Elizondo G, Hahn PF, Saini S, Todd LE, et al. Superparamagnetic iron oxide: clinical application as a contrast agent for MR imaging of the liver. Radiology. 1988; 168(2):297–301.
20. Asahina Y, Izumi N, Uchihara M, Noguchi O, Ueda K, Inoue K, et al. Assessment of Kupffer cells by ferumoxides-enhanced MR imaging is beneficial for diagnosis of hepatocellular carcinoma: comparison of pathological diagnosis and perfusion patterns assessed by CT hepatic arteriography and CT arterioportography. Hepatol Res. 2003;27(3):196–204.
21. Imai Y, Murakami T, Yoshida S, Nishikawa M, Ohsawa M, Tokunaga K, et al. Superparamagnetic iron oxide-enhanced magnetic resonance images of hepatocellular carcinoma: correlation with histological grading. Hepatology. 2000;32(2):205–12.
22. Blomley MJ, Albrecht T, Cosgrove DO, Patel N, Jayaram V, Butler-Barnes J, et al. Improved imaging of liver metastases with stimulated acoustic emission in the late phase of enhancement with the US contrast agent SH U 508A: early experience. Radiology. 1999;210(2):409–16.
23. Numata K, Morimoto M, Ogura T, Sugimori K, Takebayashi S, Okada M, et al. Ablation therapy guided by contrast-enhanced sonography with Sonazoid for hepatocellular carcinoma lesions not detected by conventional sonography. J Ultrasound Med. 2008;27(3):395–406.
24. Luo W, Numata K, Morimoto M, Kondo M, Takebayashi S, Okada M, et al. Focal liver tumors: characterization with 3D perflubutane microbubble contrast agent-enhanced US versus 3D contrast-enhanced multidetector CT. Radiology. 2009;251(1):287–95.
25. Kudo M. New sonographic techniques for the diagnosis and treatment of hepatocellular carcinoma. Hepatol Res. 2007; 37(Suppl 2):S193–9.
26. Hohmann J, Albrecht T, Hoffmann CW, Wolf KJ. Ultrasonographic detection of focal liver lesions: increased sensitivity and

specificity with microbubble contrast agents. Eur J Radiol. 2003;46(2):147–59.
27. Hirokawa Y, Isoda H, Maetani YS, Arizono S, Shimada K, Okada T, et al. Hepatic lesions: improved image quality and detection with the periodically rotated overlapping parallel lines with enhanced reconstruction technique—evaluation of SPIO-enhanced T2-weighted MR images. Radiology. 2009;251(2): 388–97.
28. Vogl TJ, Schwarz W, Blume S, Pietsch M, Shamsi K, Franz M, et al. Preoperative evaluation of malignant liver tumors: comparison of unenhanced and SPIO (Resovist)-enhanced MR imaging with biphasic CTAP and intraoperative US. Eur Radiol. 2003;13(2):262–72.
29. Edey AJ, Ryan SM, Beese RC, Gordon P, Sidhu PS. Ultrasound imaging of liver metastases in the delayed parenchymal phase following administration of Sonazoid using a destructive mode technique (Agent Detection Imaging). Clin Radiol. 2008;63(10): 1112–20.
30. Kudo M. Will Gd-EOB-MRI change the diagnostic algorithm in hepatocellular carcinoma? Oncology. 2010;78(Suppl 1):87–93.

CME

Open

Radiofrequency Ablation for Hepatocellular Carcinoma: 10-Year Outcome and Prognostic Factors

LIVER

Shuichiro Shiina, MD, PhD[1], Ryosuke Tateishi, MD, PhD[1], Toru Arano, MD[1], Koji Uchino, MD[1], Kenichiro Enooku, MD, PhD[1], Hayato Nakagawa, MD, PhD[1], Yoshinari Asaoka, MD, PhD[1], Takahisa Sato, MD, PhD[1], Ryota Masuzaki, MD, PhD[1], Yuji Kondo, MD, PhD, Tadashi Goto, MD, PhD[1], Haruhiko Yoshida, MD, PhD[1], Masao Omata, MD, PhD[1] and Kazuhiko Koike, MD, PhD[1]

OBJECTIVES: **Radiofrequency ablation (RFA) is widely performed for hepatocellular carcinoma (HCC). However, there has been no report on 10-year outcome of RFA. The objective of this study was to report a 10-year consecutive case series at a tertiary referral center.**

METHODS: **We performed 2,982 RFA treatments on 1,170 primary HCC patients and analyzed a collected database.**

RESULTS: **Final computed tomography images showed complete tumor ablation in 2,964 (99.4%) of 2,982 treatments performed for the 1,170 primary HCC patients. With a median follow-up of 38.2 months, 5- and 10-year survival rates were 60.2% (95% confidence interval (CI): 56.7–63.9%) and 27.3% (95% CI: 21.5–34.7%), respectively. Multivariate analysis demonstrated that age, antibody to hepatitis C virus (anti-HCV), Child-Pugh class, tumor size, tumor number, serum des-γ-carboxy-prothrombin (DCP) level, and serum lectin-reactive α-fetoprotein level (AFP-L3) were significantly related to survival. Five- and 10-year local tumor progression rates were both 3.2% (95% CI: 2.1–4.3%). Serum DCP level alone was significantly related to local tumor progression. Five- and 10-year distant recurrence rates were 74.8% (95% CI: 71.8–77.8%) and 80.8% (95% CI: 77.4–84.3%), respectively. Anti-HCV, Child-Pugh class, platelet count, tumor size, tumor number, serum AFP level, and serum DCP level were significantly related to distant recurrence. There were 67 complications (2.2%) and 1 death (0.03%).**

CONCLUSIONS: **RFA could be locally curative for HCC, resulting in survival for as long as 10 years, and was a safe procedure. RFA might be a first-line treatment for selected patients with early-stage HCC.**

SUPPLEMENTARY MATERIAL is linked to the online version of the paper at http://www.nature.com/ajg

Am J Gastroenterol 2012; 107:569–577; doi:10.1038/ajg.2011.425; published online 13 December 2011

INTRODUCTION

Hepatocellular carcinoma (HCC) is the fifth most common malignant neoplasm in the world (1). Only 20% of HCC patients are candidates for resection (2). Furthermore, recurrence is frequent even after apparently curative resection. Liver transplantation is restricted by organ donor shortage. Thus, various nonsurgical therapies have been introduced (3–5). Among these, image-guided percutaneous ablation is considered best for early-stage HCC.

Ethanol injection was formerly the standard procedure among the various percutaneous ablation techniques. Randomized controlled trials, however, have demonstrated that radiofrequency ablation (RFA) has a more reliable local antitumor effect, leading to a lower local tumor progression risk and higher survival rates (6–9). RFA has largely replaced ethanol injection (10).

Several reports on 5-year outcome of RFA exist (11–17); however, no study has covered 10-year outcome. We report on a 10-year consecutive case series at a tertiary referral center. We analyzed antitumor effect, patient survival, local tumor progression, and distant recurrence rates, variables relevant to these outcomes, and complications. To our knowledge, this study documents the largest number of RFA treatments performed at a single institution.

METHODS

RFA indications

RFA was the treatment of choice in HCC patients satisfying the following criteria: (i) ineligible for surgical resection/liver transplantation or patient refusal for surgery; (ii) no extrahepatic metastasis/vascular invasion; and (iii) no other malignancies that

[1]Department of Gastroenterology, Graduate School of Medicine, The University of Tokyo, Tokyo, Japan. **Correspondence:** Shuichiro Shiina, MD, PhD, Department of Gastroenterology, Graduate School of Medicine, The University of Tokyo, 7-3-1, Hongo, Bunkyo-ku, Tokyo 113-8655, Japan. E-mail: sshiina-tky@umin.ac.jp
Received 8 May 2011; accepted 5 November 2011

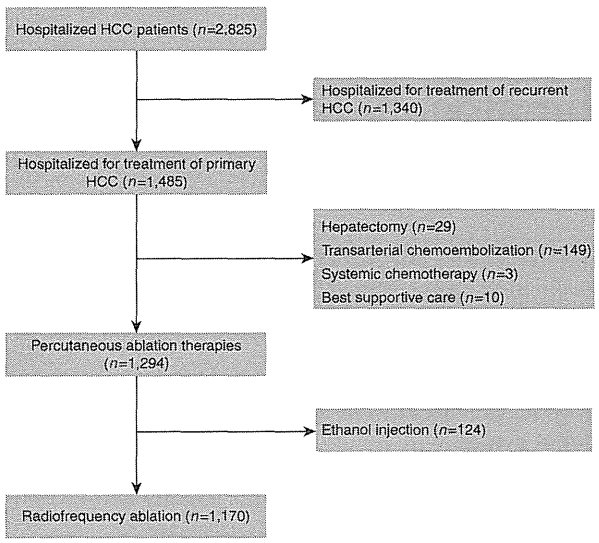

Figure 1. Flow of patients in this study. HCC, hepatocellular carcinoma.

may determine the patient's prognosis. Exclusion criteria were as follows: (i) tumor not visualized by ultrasonography/not accessible percutaneously; (ii) total bilirubin level ≥3.0 mg/dl; (iii) platelet count $< 50\times10^9$/l or prothrombin activity < 50%; (iv) refractory ascites; (v) enterobiliary reflux; and (vi) adhesion between the tumor and the gastrointestinal tract. In general, we performed RFA on Child-Pugh class A or B patients, a single tumor ≤5 cm in diameter, or three or fewer tumors ≤3 cm in diameter. In cases beyond these conditions, we performed RFA on patients who were likely to benefit from this procedure for possible cure or prolongation of life. No patients were excluded solely on account of tumor location (18). Informed consent was obtained from each patient. This study was conducted according to the ethical guidelines of the 1975 Declaration of Helsinki and approved by the institutional review board (Registration ID: P98C05-11Y).

Patients

In this cohort study, we analyzed a prospectively collected computerized database. Between February 1999 and December 2009, 2,825 HCC patients were admitted once or more to the Department of Gastroenterology, the University of Tokyo (**Figure 1**). At initial hospitalization, 1,485 had primary HCC and the remaining 1,340 had recurrent HCC. In the recurrent HCC patients, primary HCC had previously been treated by therapies other than RFA.

Of the 1,485 primary HCC patients, 1,294 (87.1%) underwent percutaneous ablation as the initial treatment, including RFA. The remaining 191 patients underwent other therapies: hepatic resection, 29 patients with good liver function and who consented to an operation; transarterial chemoembolization, 149 with multinodular or large tumors that could not be treated by ablation therapies; systemic chemotherapy, three with extrahepatic metastasis; and only supportive care, 10 with decompensated cirrhosis or poor general condition.

Of the 1,294 patients treated by percutaneous ablation, 1,170 underwent RFA and the other 124 underwent ethanol injection. The choice of therapy was made as follows: between April 1999 and January 2001, 232 patients with three or fewer tumors, each ≤3 cm in diameter, and Child-Pugh class A or B liver function were entered into a randomized controlled trial to compare RFA with ethanol injection (6). Patients outside these inclusion criteria were mostly treated by RFA. After this trial, RFA was generally the treatment of choice, and ethanol injection was administered only to those considered unsuitable for RFA; ethanol injection was administered to those with either enterobiliary reflux or adhesion of the tumor to the gastrointestinal tract.

HCC was diagnosed based on typical imaging findings; that is, early-phase enhancement and late-phase contrast washout on dynamic computed tomography (CT) (19). HCC diagnosis was also confirmed by biopsy in 1,078 (92.1%) of the 1,170 patients with RFA-treated primary HCC. A total of 998 (85.3%) were diagnosed as having liver cirrhosis.

In general, transarterial chemoembolization was combined with RFA in patients with either ≥4 tumors or those with even one tumor >3.0 cm in diameter, although indication criteria of this combination had changed over time. The combination of transarterial chemoembolization with RFA was performed in 324 primary HCC patients.

Treatment methods

RFA was performed on an inpatient basis. Preoperative planning including evaluation of all imaging studies, and careful ultrasound examination was performed to identify the tumors and determine the access routes.

The procedure was performed according to an institutional protocol and in the presence of three physicians. One physician inserted the electrode under ultrasound guidance while another assisted the procedure; at least one had 8-year or longer experience of percutaneous ablation therapies. The remaining physician was responsible for the ultrasound machine and data recording. Video recording was performed occasionally to improve and standardize the procedure.

The precise techniques of RFA are described elsewhere (6). Briefly, all RFA procedures were performed percutaneously under ultrasound guidance (Power Vision 8000, Aplio XV or Aplio XG; Toshiba, Tokyo, Japan). We used artificial pleural effusion (20) or artificial ascites (21) for tumors, which were in the hepatic dome or adjacent to the gastrointestinal tract. After administration of sedatives and local anesthesia, a 17-gauge cooled-tip electrode (Cool-Tip; RF Ablation System, Covidien, Boulder, Colombia, CO) was inserted. Radiofrequency energy was delivered for 6–12 min for each application. For large tumors, the electrode was repeatedly inserted into different sites, such that the entire tumor could be enveloped by assumed necrotic volumes. Following the procedure, the patient remained in bed until the next morning.

A CT scan with a 5-mm section thickness was performed 1–3 days after RFA to evaluate technique effectiveness (22). Complete ablation was defined as hypoattenuation of the entire tumor. We intended to ablate not only the tumor but also some of the liver

parenchyma surrounding it. When we suspected that unablated tumor portions remained, the procedure was repeated. We did not predefine the procedure number in a treatment: treatment was generally continued until CT imaging demonstrated necrosis of the entire tumor.

Follow-up

To detect recurrence at an early stage, serum α-fetoprotein (AFP), lectin-reactive AFP (AFP-L3), and des-γ-carboxy-prothrombin (DCP) levels were measured monthly, and CT and ultrasonography were performed every 4 months. Local tumor progression was defined as the appearance of viable cancer tissue touching the initially treated tumor (22) and distant recurrence as the emergence of one or several tumor(s) separate from the primary site. Chest CT or bone scintigraphy was performed if extrahepatic recurrence was suspected. RFA was used for recurrence if the patient still met the indication criteria. If multiple recurrences were not treatable with RFA, transarterial chemoembolization was generally performed.

Statistical analysis

This is a report of a consecutive case series: all RFA treatments performed on primary HCC patients at the Department of Gastroenterology, University of Tokyo between February 1999 and December 2009 were included and none was excluded. Data are presented as mean±s.d. for quantitative variables, and as absolute frequencies for qualitative variables.

A "procedure" was defined as a single intervention episode comprising one or more ablation performed on one or more tumors and a "treatment" as the completed effort to ablate one or more tumors. A treatment comprised one or more procedures (22).

"Technique effectiveness" rate was defined as the percentage of successfully eradicated macroscopic tumors, as evidenced by CT scan 1–3 days after the last procedure (22).

Overall survival was calculated in the 1,170 primary HCC patients. Survival curves were generated by the Kaplan–Meier method. In addition to overall survival, some subgroup analyses were performed with clinical characteristics including tumor size, tumor number, and liver function. Recurrence was evaluated in 1,138 of the 1,170 primary HCC patients; the remaining 32 patients were excluded from the recurrence analysis because some small tumors had been left untreated by RFA on account of detection failure by ultrasonography. Recurrence rates were calculated by the Gaynor's method (23). All time estimates were made from the date of the first RFA. The follow-up was finalized at either death or the last visit to the outpatient clinic before 31 December 2009. Transplanted patients were censored from this study at the date of transplantation.

The prognostic relevance of 19 baseline variables (**Table 1**), the combination of transcatheter arterial chemoembolization (TACE) with RFA, HCC recurrence, and the number of RFA sessions to survival was analyzed by univariate and multivariate Cox proportional hazards regression models. The prognostic relevance of 19 baseline variables (**Table 1**), the combination of TACE with RFA, and the number of RFA sessions to local tumor progression and distant recurrence was also analyzed by univariate and multivariate models. All variables with a P value <0.05 by univariate comparison were subjected to multivariate analysis. Some continuous variables in which log-linearity could not be assumed were transformed into categorical variables. In multivariate analysis, we evaluated two models that contained either Child-Pugh class or its components to avoid multicollinearity. A stepwise variable selection was performed with Akaike Information Criteria in multivariate analysis. The results of multivariate analyses were presented as a hazard ratio with corresponding 95% confidence interval (CI), with P values from the Wald test. All significance tests were two-tailed, and differences with a P value <0.05 were considered statistically significant.

Complications were defined according to the guidelines of the Society of Interventional Radiology (24).

RESULTS

Antitumor effect

We performed a total of 2,982 RFA treatments for the 1,170 primary HCC patients, comprising 4,514 procedures. Thus, procedure number per treatment was 1.52±0.78. Many patients undergoing RFA for treatment of primary HCC received iterative RFA treatments for recurrence. A total of 485 patients underwent RFA treatment once, 247 twice, 177 thrice, 94 four times, 70 five times, 35 six times, 23 seven times, 14 eight times, 7 nine times, 7 ten times, 6 eleven times, 2 twelve times, 2 thirteen times, and 1 fourteen times.

Technique effectiveness rate was 99.4% (2,964/2,982 treatments). It was similar between the initial RFA treatments and the other RFA treatments for recurrence ($P=0.98$). Complete ablation of the tumor was achieved in 1,163 (99.4%) of the 1,170 initial treatments and in 1,801 (99.4%) of the 1,812 other RFA treatments. However, technique effectiveness rate significantly differed with tumor size ($P=0.023$). No apparent viable portions remained in the treated tumor in 1,642 (99.6%) of 1,648 treatments for tumors ≤2.0 cm in diameter, in 923 (99.2%) of 930 treatments for tumors 2.1–3.0 cm, in 356 (98.9%) of 360 treatments for tumors 3.1–5.0 cm, and in 43 (97.7%) of 44 treatments for tumors >5.0 cm. Final CT imaging demonstrated residual cancer tissue in the remaining 18 treatments. We decided against performing additional procedures, because liver failure rather than HCC seemed to determine the prognosis in 10 treatments, and because additional RFA would have caused complications on account of poor visualization or inaccessibility in the other eight treatments.

Survival

The 19 baseline clinical characteristics of the 1,170 patients who underwent RFA for treatment of primary HCC are shown in **Table 1**. A total of 269 patients (23.0%) were >75 years old. In all, 422 patients had tumors ≤2.0 cm in diameter, 467 had tumors 2.1–3.0 cm, 246 had tumors 3.1–5.0 cm, and 35 had tumors >5.0 cm; 685 patients had 1 tumor, 395 had 2 or 3 tumors, and 90 had ≥4 tumors.

As of December 2009 (with a median follow-up of 38.2 months), 692 patients (59.1%) remained alive, 39 (3.3%) were lost to

Table 1. Baseline characteristics of the 1,170 patients undergoing radiofrequency ablation for primary hepatocellular carcinoma

Variable	
Age (years)	68.3±8.6
Males, *n* (%)	751 (64.1)
Viral infection	
HBs-Ag-positive, *n* (%)	127 (10.9)
Anti-HCV-positive, *n* (%)	870 (74.4)
Both positive, *n* (%)	13 (1.1)
Both negative, *n* (%)	159 (13.6)
Alcohol consumption >80 g/d	170 (14.5)
Ascites, *n* (%)	117 (10.0)
Encephalopathy, *n* (%)	24 (2.1)
Albumin (g/dl)	3.65±0.47
Total bilirubin (mg/dl)	0.95±0.49
Prothrombin time (%)	79.6±14.1
Platelet count (×10⁴/mm³)	11.9±5.6
AST (IU/l)	61.5±35.9
ALT (IU/l)	57.3±40.8
Child-Pugh class, n *(%)*	
A	868 (74.2)
B	291 (24.9)
C	11 (0.9)
Tumor size (cm)	2.54±1.04
Tumor number	1.8±1.2
Serum AFP (ng/dl), n *(%)*	
≤100	928 (793)
101–400	146 (12.5)
>400	96 (8.2)
Serum DCP (mAU/ml), n *(%)*[a]	
≤100	964 (83.1)
101–400	126 (10.9)
>400	70 (6.0)
Serum AFP-L3 (%), n *(%)*	
≤15	1,015 (86.8)
15.1–40	74 (6.3)
>40	81 (6.9)

AFP, α-fetoprotein; AFP-L3, lectin-reactive α-fetoprotein; ALT, alanine aminotransferase; AST, asparatate aminotransferase; DCP, des-γ-carboxy-prothrombin; HCV, hepatitis C virus.

Data are expressed as mean±s.d.

[a]Serum DCP level could not be measured in 10 patients because they were being administered warfarin.

Figure 2. Overall survival in 1,170 primary hepatocellular carcinoma patients who underwent radiofrequency ablation.

follow-up, and 439 (37.5%) had died. Of the 1,170 patients, two were transplanted. The number of 5-, 7-, and 10-year survivors was 325, 131, and 16, respectively. The cause of death was HCC in 245 patients (55.8%), liver failure in 89 (20.3%), upper gastrointestinal bleeding in 11 (2.5%), complications related to the procedure in 3 (0.7%), liver-unrelated diseases in 81 (18.5%), and undetermined in 10 (2.3%).

The 1-, 3-, 5-, 7-, and 10-year survival rates of all 1,170 primary HCC patients were 96.6% (95% CI: 95.5–97.7%), 80.5% (95% CI: 78.0–83.1%), 60.2% (95% CI: 56.7–63.9%), 45.1% (95% CI: 40.9–49.6%), and 27.3% (95% CI: 21.5–34.7%), respectively (**Figure 2**; **Table 2**). Survival rates differed significantly with tumor size ($P<0.0001$), tumor number ($P=0.0003$), and Child-Pugh class ($P<0.0001$). In the Child-Pugh class A or B patients with a single tumor ≤5 cm in diameter, or three or fewer tumors ≤3 cm in diameter, the 5-year survival rate was 63.8% (95% CI: 59.9–67.9%), while in those outside these criteria, it was 46.4% (95% CI: 39.4–54.8%).

Univariate analysis showed 19 of the 22 variables relevant to survival. In multivariate analysis that contained Child-Pugh class but not its components, a model that contained age, antibody to hepatitis C virus (anti-HCV), Child-Pugh class, tumor size, tumor number, serum DCP level, and serum AFP-L3 level was selected (**Table 3**). The other model that contained the components of Child-Pugh class is shown in **Supplementary Table** online.

Recurrence

Recurrence developed in 741 patients. Local tumor progression alone was found in 25, local tumor progression with distant recurrence was found in 9, and distant recurrence alone was found in the other 707 patients. Of these 707 patients, 13 had the first recurrence in extrahepatic sites: 7 had lymph node metastasis, 3 had peritoneal seeding, 1 had lung metastasis, 1 had bone metastasis, and the remainder had both peritoneal seeding and lung metastasis. No recurrence developed in the remaining 397 patients.

Of the 741 patients, the first recurrence was treated by iterative RFA in 659 (88.9%), transarterial chemoembolization in 69 (9.3%), systemic chemotherapy in 4 (0.5%), surgical resection in 3 (0.4%), radiation therapy in 2 (0.3%), and supportive care in 4 (0.5%).

Table 2. Survival of patients undergoing radiofrequency ablation, based on tumor number, tumor size, and Child-Pugh class

Grading	*n*	Survival (%)					Median (years)	*P* value
		1-Year	3-Year	5-Year	7-Year	10-Year		
Overall survival	1,170	96.6	80.5	60.2	45.1	27.3	6.4	—
Tumor number								
Solitary	685	97.2	82.6	64.6	50.5	32.0	7.0	0.0003
2–3	395	95.7	77.9	54.4	39.4	19.9	5.6	
≥4	90	96.5	76.4	53.6	30.1	17.6	5.3	
Tumor size								
≤3 cm	889	97.2	83.8	65.1	47.3	30.7	6.7	<0.0001
>3 cm	281	94.8	71.0	46.5	38.0	18.6	4.6	
Child-Pugh class								
A	868	98.0	86.0	65.9	50.2	30.1	7.0	<0.0001
B	291	93.2	66.4	46.5	32.4	20.6	4.6	
C	11	81.8	58.4	23.4	23.4	—	3.1	
Combination of tumor number, tumor size, and Child-Pugh class								
Solitary, ≤3 cm	534	97.6	84.7	68.0	51.4	34.3	7.1	—
Solitary, ≤3 cm, Child-Pugh A	401	98.7	90.1	74.0	57.4	41.3	8.2	—
1–3 Tumors, ≤3 cm	822	97.1	83.7	65.2	48.8	32.5	6.9	—
Solitary, ≤5 cm, or 1–3 tumors, ≤3 cm	947	97.2	82.8	63.8	48.8	30.6	6.9	—
Child-Pugh A/B								
Satisfied the indication criteria of surgical resection proposed in the BCLC protocol[a]	237	98.6	90.5	75.9	61.1	38.1	8.7	—

BCLC, Barcelona Clinic Liver Cancer; HCC, hepatocellular carcinoma.
[a]Child-Pugh class A with a normal level of bilirubin, no significant portal hypertension, and a single HCC.

The 1-, 3-, 5-, 7-, and 10-year rates of local tumor progression with or without distant recurrence were 1.4% (95% CI: 0.7–2.1%), 3.2% (95% CI: 2.1–4.3%), 3.2% (95% CI: 2.1–4.3%), 3.2% (95% CI: 2.1–4.3%), and 3.2% (95% CI: 2.1–4.3%), respectively (**Figure 3**). Univariate analysis demonstrated that prothrombin time and serum AFP, DCP, and AFP-L3 levels were correlated to local tumor progression, whereas multivariate analysis showed that serum DCP level alone was significantly correlated. Tumor size was not correlated to local tumor progression.

The 1-, 3-, 5-, 7-, and 10-year rates of distant recurrence without local tumor progression were 25.6% (95% CI: 23.0–28.2%), 63.3% (95% CI: 60.2–66.4%), 74.8% (95% CI: 71.8–77.8%), 78.1% (95% CI: 75.1–81.2%), and 80.8% (95% CI: 77.4–84.3%), respectively. Univariate analysis demonstrated 14 variables relevant to distant recurrence, whereas multivariate analysis showed that anti-HCV, Child-Pugh class, platelet count, tumor size, tumor number, serum AFP level, and serum DCP level were significantly related to distant recurrence (**Table 3**).

Complications

A total of 67 complications were encountered (**Table 4**). The incidence rates of complications per treatment and per procedure were 2.2% (67/2,982) and 1.5% (67/4,514), respectively. One patient died of hepatic failure on account of massive hepatic infarction 7 days after the last RFA procedure. He had undergone 12 RFA treatments in 8 years. The treatment mortality rate was 0.03%.

DISCUSSION

This study describes our 10-year clinical experience with RFA at a high-volume center. We performed the 2,982 RFA treatments on a total of the 1,170 primary HCC patients, showing that RFA has a high antitumor effect. Tumors were judged to have been completely ablated by final CT imaging in 99.4% of the treatments. Complete response was achieved not only in the first RFA but also in iterative RFA for recurrence. Although complete response rate differed with tumor size, there was not a sharp drop-off in effectiveness. The complete response rate may be higher in this study than others probably because we generally repeated the procedure until CT imaging demonstrated complete tumor necrosis, whereas many other studies limited the procedure number of RFA to 2–3 (11,13,15). Complete ablation of tumors has been reported to be related to improved survival (25). There were the 18 treatments in which we did not perform additional RFA for residual cancer tissue. In those treatments, usefulness of RFA had been unclear at the initial session because of liver dysfunction or tumor burden.